

LMU-Based Sequential Learning and Posterior Ensemble Fusion for Cross-Domain Infant Cry Classification

Niloofar Jazaeri
University of Ottawa
Ottawa, Canada
njaza024@uottawa.ca

Hilmi R. Dajani
University of Ottawa
Ottawa, Canada
hdajani@uottawa.ca

Marco Janeczek
Crynostics Inc.
Canada
marco@crynostics.com

Martin Bouchard
University of Ottawa
Ottawa, Canada
bouchm@uottawa.ca

Abstract—Decoding infant cry causes remains challenging for healthcare monitoring due to short nonstationary signals, limited annotations, and strong domain shifts across infants and datasets. We propose a compact acoustic framework that fuses MFCC, STFT, and pitch features within a multi-branch CNN encoder and models temporal dynamics using an enhanced Legendre Memory Unit (LMU). Compared to LSTMs, the LMU backbone provides stable sequence modeling with substantially fewer recurrent parameters, supporting efficient deployment. To improve cross-dataset generalization, we introduce calibrated posterior ensemble fusion with entropy-gated weighting to preserve domain-specific expertise while mitigating dataset bias. Experiments on Baby2020 and Baby_Crying demonstrate improved macro-F1 under cross-domain evaluation, along with leakage-aware splits and real-time feasibility for on-device monitoring.

Index Terms—Infant cry, Legendre memory unit, sequential learning, ensemble learning, posterior fusion, domain adaptation.

I. INTRODUCTION

Infant cry is one of the earliest and most informative communication signals between newborns and caregivers. Accurately decoding cry causes (e.g., hunger, discomfort, pain) can improve parental responsiveness and provide non-invasive clinical cues for early detection of pathological conditions [1]–[3]. However, even experienced caregivers struggle to reliably distinguish acoustic nuances, and expert annotation is costly and inconsistent, motivating machine listening systems that can robustly interpret infant cries across diverse settings.

Despite progress, cry analysis remains challenging. Cries are short, nonstationary, and highly variable across infants and sessions. The datasets are small and imbalanced, and they are prone to overestimation due to *leakage*—where portions of segments or augmented cry samples from the same cry appear in both the training and test sets. Environmental variability such as background noise, overlapping speech, and sounds from television further undermines generalization. Prior work on cry detection in naturalistic conditions [4] and infant monitoring systems [5] highlighted how acoustic interference

severely reduces system reliability, underscoring the need for models resilient to domain shift. Cry-cause classification is particularly sensitive, as it requires capturing fine-grained spectral and prosodic dynamics beyond simple cry/non-cry detection.

A broad spectrum of methodologies has been explored in prior work. Early efforts used classical machine learning such as SVMs, Random Forests, and ensemble trees on handcrafted features [6], [7], sometimes combined with transfer learning for robustness. Multi-stream classifiers have improved performance by fusing complementary acoustic views [8], [9], but most ensembles operate at the feature or decision level without addressing domain mismatch. Deep learning has since become dominant: CNNs, RNNs, and CNN–LSTM hybrids model spectro-temporal dependencies [10], [11], while ResNet and EfficientNet backbones have been benchmarked for infant cry detection [12]. More advanced approaches exploit graph neural networks [13], attention-based layers [14], ontology-driven representation learning [15], or Whisper encoder features [16]. Recent surveys highlight contrastive and multi-stream pipelines as emerging trends in cry representation learning [11]. However, while ensemble methods have been used to combine modalities or feature sets, they have not been systematically explored for *domain adaptation within the same acoustic modality*, where differences in labeling practices and acoustic environments create cross-dataset inconsistencies.

Parallel advances in self-supervised and contextualized audio representation learning further broaden the landscape. Conformer-based contrastive learning [17], contextualized acoustic embeddings [18], and compositional or contrastive cry representations [19] show promise for leveraging unlabeled audio. Domain-specific embeddings, such as neonatal health monitoring pipelines, point toward clinically viable applications, while multi-microphone separation [20] strengthens robustness under noisy conditions.

While LSTMs and GRUs remain a dominant recurrent backbone, their reliance on multiple gates makes them parameter-heavy and prone to training instabilities over long sequences [21]. The recently proposed *Legendre Memory Unit* (LMU) [22], by contrast, formulates recurrent memory as a

This work was supported by a Discovery Grant from the Natural Sciences and Engineering Research Council of Canada (NSERC) and by a MITACS Accelerate internship.

state-space projection onto orthogonal Legendre polynomials. LMUs propagate gradients stably, provide explicit control over memory span, and require up to an order of magnitude fewer parameters than LSTMs and GRUs, making them particularly suitable for lightweight, on-device cry analysis.

In this work, we make four key contributions. (1) We introduce a compact, time-preserving encoder fused with an LMU sequence model, achieving comparable or superior performance to LSTMs with significantly fewer recurrent parameters. (2) We establish a *leakage-aware evaluation protocol* to ensure unbiased training and testing across infant datasets. (3) We propose a *calibrated posterior fusion ensemble* with entropy-weighted averaging, a novel approach to domain adaptation that, unlike prior ensemble work [8], [9], explicitly handles cross-dataset inconsistency while preserving minority-class information. (4) We validate our framework for *real-time mobile deployment*, showing that lightweight models (~ 5 MB) run within ~ 3 s per 10 s cry clip, demonstrating feasibility for on-device pediatric monitoring.

II. DATASETS AND ETHICS

We evaluate our framework on two publicly available infant cry corpora. Following critiques of overestimation due to sample leakage [4], [5], all splits are leakage-safe, ensuring no baby or session overlap across training, validation, and test sets. A summary of the key properties of both datasets is provided in Table I.

Baby2020 [13]. We focus on the 0–3 months subset, containing 2,190 recordings (1–7 s, sampling frequency 16 kHz) labeled as *hungry* (590), *sleepy* (1,000), or *awake* (600). The *awake* class often captures transitional cries between sleep cycles. Recordings follow a structured naming convention (e.g., `Hungry04MB00011_2_002.wav`), where *infant age/sex* and *segment indices* are encoded. Parents provided continuous recordings, later segmented into labeled events by Ji *et al.* [13]. This dataset has become a benchmark for structured cry modeling in CNN+GNN and attention-based pipelines [13], [14]. Baby2020 dataset was recorded using caregiver-owned mobile phones and labeled by parents or caregivers, then curated and segmented under laboratory-controlled protocols. In this study, all data are split in a leakage-safe manner with no baby or session overlap across training, validation, and test sets.

Baby_Crying [23]. This dataset comprises 371 recordings with more diverse acoustic conditions than Baby2020. Durations range from 7–30 s (avg. 20 s), sampling rates vary (16 kHz most common), and background noise is moderate. Categories include *awake* (128), *uncomfortable* (128) *diaper* (134), *hungry* (160), and *sleepy* (115). Unlike Baby2020, only session-level IDs are provided, underscoring annotation and acoustic differences noted in recent surveys [11]. While less studied, this dataset complements Baby2020 by adding culturally and environmentally distinct cry samples.

TABLE I
SUMMARY OF DATASETS USED IN THIS STUDY (LEAKAGE-FREE SPLITS).

Property	Baby2020	Baby_Crying
Recordings	2,190	371
Duration (s)	1–7	7–30 (avg. ~ 20)
Noise level	Low	Moderate
Sample rate	16 kHz	Resampled to 16 kHz
ID granularity	Baby+Session	Session
Classes	3	5

III. METHODOLOGY

A. Feature Extraction

We extract four complementary acoustic representations—MFCC, STFT, F0 with confidence, and waveform energy—to capture spectral, cepstral, prosodic, and amplitude cues. Their joint utility is confirmed in ablation studies (§V).

MFCC. We compute $D=13$ mel-frequency cepstral coefficients (MFCCs) per frame using a 30 ms Hamming window and 10 ms hop size. Let $X(k, n)$ denote the short-time Fourier transform (STFT) of the signal, where $k \in \{0, \dots, K-1\}$ indexes discrete DFT frequency bins and $n \in \{1, \dots, N\}$ indexes analysis frames. The power spectrum $|X(k, n)|^2$ is passed through M triangular mel filters banks $\{H_m(k)\}_{m=1}^M$, each emphasizing energy within a specific mel-spaced frequency band. The energy in the m -th mel band at frame n is computed as

$$E_m(n) = \sum_{k=0}^{K-1} |X(k, n)|^2 H_m(k), \quad (1)$$

where $E_m(n)$ represents the total spectral energy captured by the m -th mel filter. Applying a discrete cosine transform (DCT) to the log energies yields the cepstral coefficients:

$$c_d(n) = \sum_{m=0}^{M-1} \log E_m(n) \cos \left[\frac{\pi d}{M} (m + 0.5) \right], \quad (2)$$

with $d \in \{0, \dots, D-1\}$ denoting the cepstral index. The MFCCs thus compactly encode the smooth spectral envelope of each frame, providing robustness to noise and minor channel variations by discarding fine-scale harmonic structure.

STFT. Log-power STFTs are computed with a 512-point FFT, 30 ms window, and 50% overlap:

$$S(k, n) = \log (|X(k, n)|^2 + \epsilon), \quad (3)$$

where ϵ is a small positive constant ($\epsilon = 10^{-10}$) added for numerical stability to avoid the logarithm of zero.

F0 and confidence (CREPE). We extract F0 contours and confidence $c(n) \in [0, 1]$ using CREPE [24]:

$$\hat{f}_0(n), c(n) = \text{CREPE}(x[n]). \quad (4)$$

Frames with low $c(n)$ are down-weighted. Prosodic cues from F0 trajectories help distinguish urgency in cries.

Waveform energy. The raw waveform $x[n]$, loaded using `librosa.load`, is used at its native floating-point amplitude scale (typically bounded in $[-1, 1]$ for PCM audio) without explicit peak or RMS normalization. The waveform is resampled in time to a fixed length of T using linear interpolation and provides amplitude and rhythmic envelope cues that complement the spectral features.

Feature fusion. Because different acoustic features (MFCC, STFT, F_0 with confidence, and waveform-based descriptors) are computed on distinct temporal grids, all feature matrices are resampled to a common frame length of T . Selecting the median frame length balances information preservation and memory efficiency—avoiding excessive zero-padding (as with the maximum length) and minimizing distortion from trimming shorter clips.

Let $F_m \in \mathbb{R}^{D_m \times T_m}$ denote the feature matrix for modality m , where D_m is the number of feature coefficients (e.g., 13 for MFCC) and T_m is the original number of temporal frames for that sample. Each matrix F_m is interpolated or down-sampled to the unified timeline of length T . For each target frame index $t \in \{1, 2, \dots, T\}$, the resampled value $\tilde{F}_m(t)$ is defined as

$$\tilde{F}_m(t) = F_m(\lfloor \alpha_m t \rfloor), \quad \alpha_m = \frac{T_m}{T}, \quad (5)$$

where α_m is the time-scaling ratio mapping the original frame index domain ($1 \dots T_m$) to the normalized domain ($1 \dots T$). This operation linearly aligns all feature modalities to a shared temporal grid, preserving relative dynamics such as cry onset, pitch contour, and amplitude fluctuations.

Time alignment (median length). All modalities are resampled to a common frame length of $T=233$, chosen as the median number of time frames across the training set. With a hop size of 15 ms and a 30 ms analysis window, $T=233$ corresponds to approximately $(T-1) \times 15 \text{ ms} \approx 3.48 \text{ s}$ between the first and last frame centers, or about $(T-1) \times 15 \text{ ms} + 30 \text{ ms} \approx 3.51 \text{ s}$ of signal coverage including the analysis window.

The time-aligned features are then concatenated along the channel (feature) dimension:

$$F_{\text{concat}} = [\tilde{F}_{\text{MFCC}}, \tilde{F}_{\text{STFT}}, \tilde{F}_{F_0+c}, \tilde{F}_{\text{wave}}], \quad (6)$$

producing a consistent tensor of shape $(273, 233)$ for every sample. Here, the first dimension (273) corresponds to the stacked feature channels: 257 frequency bins from the STFT magnitude spectrum, 13 MFCC coefficients, one scalar for the estimated fundamental frequency (F_0), one for the confidence score of F_0 , and one waveform-derived amplitude descriptor. The second dimension (233) represents the unified temporal frame length, corresponding to the median number of analysis windows across all cry samples. This composite (273×233) representation therefore encodes both fine-grained spectral information and longer-term prosodic cues, ensuring that all modalities remain temporally synchronized and safely reshaped for downstream CNN-LMU modeling while preserving the temporal integrity of the cry signal.

B. Encoder & Feature Fusion

Each cry sample is represented as a 233×273 matrix. A CNN stem with three Convolutional - batch normalization - pooling blocks (128, 64, 32 filters) extracts spectro-temporal patterns, following prior cry spectrogram pipelines [11], [13]. Kernel sizes capture both fine harmonics and broader shifts, with dropout and L2 regularization reducing overfitting. The output is flattened per frame to preserve temporal order for sequence modeling.

C. Sequential Memory Models: LSTM vs. LMU

Legendre Memory Unit (LMU). The LMU [22] implements recurrent memory as a continuous-time state-space system that projects recent input samples onto a fixed set of orthogonal Legendre polynomial basis functions over a temporal window θ . At each discrete timestep t , the network receives an input vector $x_t \in \mathbb{R}^p$ and maintains a linear memory state $m_t \in \mathbb{R}^d$, where d denotes the *memory order* (i.e., the number of Legendre basis functions representing the recent history). The hidden activation (readout) is $h_t \in \mathbb{R}^r$.

The discretized LMU dynamics are defined as:

$$m_{t+1} = \bar{\mathbf{A}} m_t + \bar{\mathbf{B}} u_t, \quad (7)$$

$$h_t = \mathbf{C} m_t + \mathbf{D} u_t, \quad (8)$$

where $(\bar{\mathbf{A}}, \bar{\mathbf{B}}, \mathbf{C}, \mathbf{D})$ are fixed matrices derived from the continuous Legendre basis and the window length θ . These matrices encode how recent input samples are projected into the orthogonal memory subspace, providing a stable and well-conditioned temporal representation.

The nonlinear input projection combines the current external input, the previous hidden activation, and the previous memory state:

$$u_t = W_x x_t + W_h h_{t-1} + W_m m_{t-1}, \quad (9)$$

where $W_x \in \mathbb{R}^{q \times p}$ maps the input features, $W_h \in \mathbb{R}^{q \times r}$ maps the recurrent hidden activations, and $W_m \in \mathbb{R}^{q \times d}$ maps the previous memory state into the input subspace. The resulting $u_t \in \mathbb{R}^q$ may optionally be passed through a nonlinearity such as \tanh function before driving the memory update. This hybrid formulation—linear memory with nonlinear input mixing—preserves long-range temporal dependencies with *order-of-magnitude fewer parameters* than gated RNNs (e.g., LSTMs and GRUs) while maintaining stable gradients over extended time horizons.

Long Short-Term Memory (LSTM). LSTMs [21] regulate information flow using three gating mechanisms—*input*, *forget*, and *output* gates—that control how new information is integrated, retained, or exposed at each timestep t . Given an input vector $x_t \in \mathbb{R}^p$ and the previous hidden activation

$h_{t-1} \in \mathbb{R}^r$, the gate activations and cell updates are computed as:

$$i_t = \sigma(W_i x_t + U_i h_{t-1} + b_i), \quad (10)$$

$$f_t = \sigma(W_f x_t + U_f h_{t-1} + b_f), \quad (11)$$

$$o_t = \sigma(W_o x_t + U_o h_{t-1} + b_o), \quad (12)$$

$$g_t = \tanh(W_c x_t + U_c h_{t-1} + b_c), \quad (13)$$

$$c_t = f_t \odot c_{t-1} + i_t \odot g_t, \quad (14)$$

$$h_t = o_t \odot \tanh(c_t). \quad (15)$$

Here, $\sigma(\cdot)$ denotes the logistic sigmoid function $\sigma(z) = 1/(1+e^{-z})$ that squashes values to $[0, 1]$ and determines gate activations, while $\tanh(\cdot)$ introduces bounded nonlinearity in the cell update. The operator \odot denotes element-wise (Hadamard) multiplication. Each $W_i, W_f, W_o, W_c \in \mathbb{R}^{r \times p}$ and $U_i, U_f, U_o, U_c \in \mathbb{R}^{r \times r}$ are weight matrices mapping input and recurrent signals, respectively, and $b_i, b_f, b_o, b_c \in \mathbb{R}^r$ are bias vectors. The internal state $c_t \in \mathbb{R}^r$ acts as the long-term memory, while $h_t \in \mathbb{R}^r$ represents the short-term (hidden) activation used for output and recurrence.

Each update involves multiple matrix multiplications, non-linear activations, and gating operations—making LSTMs highly expressive but relatively heavy in parameters and computational cost.

Comparison. Unlike LSTMs, which learn all recurrent weights, LMUs employ fixed orthogonal memory dynamics with a learned readout layer, achieving approximately 95% fewer recurrent parameters [22]. This design yields faster training, lower inference latency, and improved numerical stability, making LMUs particularly suitable for mobile and real-time deployment, whereas LSTMs remain competitive for strongly nonlinear or event-driven temporal dynamics.

D. Domain Adaptation via Calibrated Posterior Fusion

We train two domain-specific classifiers: one on Baby2020 with labels *hug*, *uncomfortable*, *sleepy* and one on Baby_Crying with labels *hungry*, *awake*, *sleepy*. At inference, their outputs are projected into a shared union label space $\mathcal{L} = \{hungry, awake, hug, uncomfortable, sleepy\}$, as shown in the workflow of Fig. 1.

Algorithmic steps. Algorithm 1 summarizes the proposed calibrated posterior fusion procedure. Each domain-specific classifier is first *temperature-calibrated* on its own validation set to correct for overconfident posterior estimates. Specifically, a positive scalar temperature parameter T_m is learned for each model m by minimizing the negative log-likelihood on the validation data. This temperature rescales the model logits before the softmax operation, producing calibrated posterior probabilities.

During inference, the temperature-calibrated logits of each classifier are projected into a shared union label space. Disjoint classes (e.g., *hungry* from Baby_Crying or *hug* from Baby2020) are inserted directly, while the shared class *sleepy* is fused across domains using a log-sum-exp operation weighted by predictive entropy. This entropy-gated weighting ensures that models with lower posterior entropy (i.e., higher

Algorithm 1 Leakage-safe training and calibrated posterior fusion across Baby2020 and Baby_Crying datasets.

Baby2020 dataset \mathcal{D}_B with labels $\{hug, uncomfortable, sleepy\}$. Baby_Crying dataset \mathcal{D}_C with labels $\{hungry, awake, sleepy\}$. Union label space $\mathcal{L} = \{hungry, awake, hug, uncomfortable, sleepy\}$.

Stage 1: Leakage-safe training For $\mathcal{D}_m \in \{\mathcal{D}_B, \mathcal{D}_C\}$: Split \mathcal{D}_m into train, validation, and test sets with no baby or session overlap. Train CNN+LMU classifier f_m with early stopping.

Stage 2: Post-hoc temperature calibration For each trained model f_m : Collect validation logits $z_m^{(n)}$ and labels $y^{(n)}$. Estimate temperature $T_m > 0$ by minimizing negative log-likelihood $T_m = \arg \min_T \left(-\sum_n \log \frac{\exp(z_m^{(n)}[y^{(n)}/T])}{\sum_j \exp(z_m^{(n)}[j]/T)} \right)$.

Stage 3: Calibrated posterior fusion (inference) For each test cry recording x : Compute calibrated posteriors $p_m(y|x, T_m) = \frac{\exp(z_m(y)/T_m)}{\sum_j \exp(z_m(j)/T_m)}$. Initialize union logits $z \in \mathbb{R}^{|\mathcal{L}|}$ with $-\infty$. Insert disjoint class logits into z . Fuse shared class (*sleepy*) via log-sum-exp:

$$z[\text{sleepy}] = \log(w_C e^{z_C[\text{sleepy}]} + w_B e^{z_B[\text{sleepy}]}).$$

Compute entropy-gated weights $w_m \propto \exp(-\tau H(p_m))$, $\sum_m w_m = 1$. Output final prediction $p^*(y|x) = \text{softmax}(z)$.

confidence after calibration) contribute more strongly to the final decision. An optional product-of-experts variant was also evaluated for the overlapping class, yielding sharper consensus when both models agree.

Illustrative examples of calibrated posterior fusion. We next highlight how calibration and entropy-gated fusion resolve conflicts across datasets.

Interpretation of calibrated posterior fusion behavior. Table II presents representative, sample-level case studies illustrating how calibrated posterior fusion combines domain-specific predictions from the Baby2020 and Baby_Crying models. Unlike the aggregate metrics reported in Section IV, these examples serve a qualitative and explanatory role, clarifying *how* temperature calibration and entropy-gated weighting influence individual decisions.

Why ensemble domain adaptation matters for baby cry. Compared to naive dataset merging, posterior fusion preserves domain-specific strengths and reduces bias. In cry classification, merging datasets can worsen class imbalance and obscure annotation differences, while majority voting fails when label spaces differ (e.g., *hungry* in Baby_Crying vs. *hug* in Baby2020). Treating each dataset as an expert and combining them only at inference through calibrated posterior fusion avoids annotation conflicts, improves minority-class representation, and broadens domain coverage without retraining. Table III quantitatively compares these domain adaptation strategies under cross-dataset evaluation.

Each case contrasts uncalibrated and calibrated fusion out-

TABLE II

REPRESENTATIVE CASE STUDIES OF CALIBRATED POSTERIOR FUSION ACROSS BABY2020 AND BABY_CRYING MODELS. MOST CASES ILLUSTRATE SUCCESSFUL CONFLICT RESOLUTION VIA CALIBRATION AND ENTROPY GATING; THE FINAL ROW HIGHLIGHTS A FAILURE CASE WHERE A HIGHLY CONFIDENT BUT INCORRECT DOMAIN PREDICTION DOMINATES.

Case	Posterior behavior and fusion outcome
Cry: Hungry (calibration effect)	Baby_Crying: hungry=0.92, sleepy=0.08. Baby2020: hug=0.60, sleepy=0.40. Without calibration: predicts hungry (overconfident). With calibration ($T_C=1.6$, $T_B=0.8$): hungry=0.70 vs. hug=0.65 \Rightarrow hungry .
Cry: Hungry (entropy gating)	Baby_Crying: hungry=0.88, sleepy=0.08, awake=0.04. Baby2020: sleepy=0.55, discomfort=0.45. Lower entropy in Baby_Crying \Rightarrow fusion favors hungry .
Cry: Hug	Baby_Crying: diffuse across hungry/awake/sleepy. Baby2020: hug=0.92 (low entropy). Fusion correctly favors Baby2020 \Rightarrow hug .
Cry: Sleepy	Baby_Crying: sleepy \sim 0.8; Baby2020: sleepy \sim 0.8. Agreement across domains \Rightarrow sleepy .
Cry: Sleepy (failure case predicted Hungry)	Baby_Crying: hungry=0.95 (very low entropy, incorrect label). Baby2020: sleepy=0.60, hug=0.40 (higher entropy, correct). Entropy gating strongly weights Baby_Crying, causing fusion to incorrectly predict as hungry .

comes. A case is considered *successful* when either (i) both domains agree with high confidence on the correct label, or (ii) calibration and entropy gating resolve cross-domain conflicts by reducing overconfidence or prioritizing the more reliable expert. Conversely, a case is *unsuccessful* when a domain-specific model dominates the ensemble due to unjustified low entropy, leading to misclassification.

The first example (*Hungry – calibration effect*) shows how temperature scaling ($T_C=1.6$, $T_B=0.8$) softens overconfident posteriors from the Baby_Crying model, enabling a more balanced fusion while preserving the correct *Hungry* prediction. The second case (*Hungry – entropy gating*) demonstrates how lower-entropy posteriors are weighted more strongly, allowing the Baby_Crying model to dominate when its prediction is confident and correct. In the third example (*Hug*), the Baby2020 model exhibits a sharp, low-entropy posterior that appropriately overrides the diffuse output of the Baby_Crying model. The fourth case (*Sleepy*) represents an ideal scenario in which both domains produce aligned, high-confidence predictions, resulting in a straightforward consensus decision.

The final row of Table II highlights a limitation of entropy-gated fusion: when a domain-specific model is confidently wrong, its low-entropy posterior can dominate the ensemble and override a more uncertain but correct prediction from the other domain. This motivates future work on uncertainty-aware rejection and dynamic domain reliability estimation.

Overall, calibrated posterior fusion improves reliability by (a) tempering overconfident probabilities through temperature scaling, (b) weighting domain contributions via predictive entropy, and (c) producing more consistent and symmetric

decisions across domains. These qualitative examples complement the quantitative evaluation in Section IV by revealing the internal decision behavior of the proposed fusion strategy.

Why this works. This calibrated fusion respects disjoint labels, combines overlap fairly, and prevents overconfident models from dominating. It allows domain expertise to be preserved without retraining, while providing flexible control through temperature scaling and entropy-based gating.

IV. EXPERIMENTS

Cry detection front-end. We adopt the cry/non-cry detector of Yao *et al.* [4], retrained and re-saved in TensorFlow 2.x for compatibility with modern Python environments (>3.8). The detector operates on 1 s analysis windows with 80% overlap and rejects non-cry acoustic events such as adult speech, background television, and silence (Fig. 2). Its computational footprint is ~ 300 MB and average latency is ~ 3 s per 10 s audio clip on an AWS CPU instance.

It is important to note that this cry-detection module is *not required* when evaluating on curated datasets such as Baby2020 or Baby_Crying, since these corpora already contain pre-segmented, clean cry samples recorded in controlled environments. However, in real-world deployment scenarios, incoming audio streams often contain long, noisy mixtures of infant and non-infant sounds. Integrating this detection stage filters out irrelevant segments and isolates cry episodes whose acoustic profiles more closely resemble the clean, laboratory-quality samples used during model training. This preprocessing step therefore bridges the gap between the model’s training conditions and field data, ensuring reliable operation in home or clinical settings where continuous recording is subject to environmental interference.

Training setup. The *Baby2020* classifier was trained for 1000 epochs with batch size 8, learning rate 10^{-3} , on 7×10 GB GPUs; the *Baby_Crying* classifier used batch size 32. Early stopping was based on macro-F1 on validation splits. Mixed-precision training was applied to reduce memory usage. The final classification model is compact (5 MB) and suitable for mobile deployment.

Feature ablation. We evaluated acoustic features extracted per cry segment, including F0 (CREPE pitch with confidence [24]), STFT, and MFCC, all resampled to a common time axis and z-scored prior to training. As shown in Table IV, the combination of MFCC and STFT achieves the highest Macro-F1 on the Baby_Crying dataset (Diaper, Sleepy, Uncomfortable), while F0 alone exhibits substantially lower discriminative power. This suggests that timbral and spectral cues dominate for these cry categories.

The contribution of pitch is more case-dependent. On Baby2020, Table V shows that combining MFCC, STFT, and F0 yields the best F1 score indicating that prosodic information can be beneficial under more structured recording conditions. Across both datasets, MFCC and STFT consistently provide the strongest discriminative cues.

Waveform energy was intentionally excluded from the Baby_Crying ablation to isolate the effect of pitch and expose

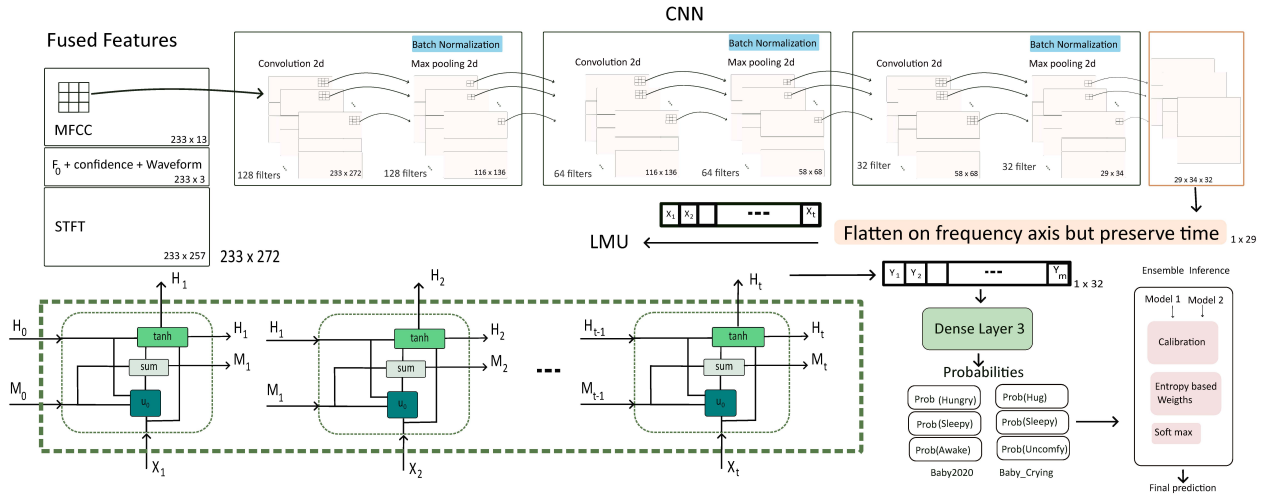


Fig. 1. Block diagram of the proposed ensemble learning approach for infant cry cause classification. Each branch integrates feature selection and sequential learning layers, and their outputs are combined using calibrated ensemble learning to enhance robustness.

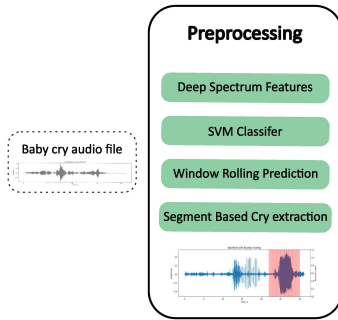


Fig. 2. Infant cry detection workflow. Non-cry segments (e.g., adult speech, middle red ribbon) are rejected. Remaining cry segments are classified into mood categories via an RBF SVM.

cases where F0 estimation becomes unreliable, such as low-energy or irregular cry segments. These observations motivate retaining the full MFCC+STFT+F0 feature set in the final model, enabling a unified preprocessing pipeline, fair comparison between ensemble and merged training strategies, and simplified real-time deployment in the iOS application.

Sequential backbone comparison. Table VI compares sequential learning models on fused features. Our CNN+LMU achieves the best trade-off, outperforming LSTM/GRU in both accuracy and efficiency, with $\sim 95\%$ fewer recurrent parameters than LSTM [22]. Compared to graph-based models [13], [14], LMU matches or exceeds performance while training faster, supporting real-time usability.

Interpretation. SOTA (*state-of-the-art*) baselines from prior literature [14], [13] represent the best published models on the Baby2020 dataset using graph-based or attention-

TABLE III

COMPARISON OF DOMAIN ADAPTATION STRATEGIES ACROSS BABY2020 AND BABY_CRYING DATASETS. RESULTS ARE MACRO-F1 (MEAN \pm STD OVER 5 RANDOM SEEDS). PROPOSED CALIBRATED FUSION YIELDS BEST CROSS-DOMAIN GENERALIZATION.

Method	Test: Baby2020	Test: Baby_Crying
Single (Baby_Crying \rightarrow Baby2020)	0.27 \pm 0.02	0.78 \pm 0.03
Single (Baby2020 \rightarrow Baby_Crying)	0.76 \pm 0.03	0.26 \pm 0.03
Majority Vote (Agree)	N/A	N/A
SoftAvg (Uncalibrated)	0.61 \pm 0.04	0.60 \pm 0.03
Calibrated Fusion (Proposed)	0.62\pm0.04	0.65\pm0.03
Merged (Joint Training)	0.58 \pm 0.05	0.55 \pm 0.04

TABLE IV

FEATURE ABLATION ON THE BABY_CRYING DATASET (DIAPER, SLEEPY, UNCOMFORTABLE). MODELS ARE TRAINED WITH AN 80% / 20% TRAIN-TEST SPLIT CNN-LSTM MODEL. WE REPORT MACRO-F1 (%). MFCC+STFT YIELDS THE STRONGEST PERFORMANCE.

Features	Macro-F1 (%)
MFCC + F0 + STFT	79.5
F0 only	46.0
MFCC only	80.0
STFT only	82.0
F0 + MFCC	78.0
F0 + STFT	80.0
MFCC + STFT	85.0

enhanced CNNs. To ensure a fair internal comparison, we re-implemented several sequential learners—LSTM, GRU, Transformer, and LMU—on top of the same CNN encoder used for feature extraction, with the same number of recurrent layers and hidden units across models (i.e., matched capacity). For each learner, only optimization parameters (learning rate, dropout, regularization) were tuned.

This controlled setup isolates the effect of the *sequential*

TABLE V
ABLATION STUDY OF ACOUSTIC FEATURES ON BABY2020 DATASETS.
METRIC: MACRO-F1 USING CNN+LSTM.

Features	F1-Score
F0 only	0.54
STFT only	0.60
MFCC only	0.58
F0 + STFT + MFCC	0.76

TABLE VI
COMPARISON OF SEQUENTIAL LEARNERS AND SOTA (*state-of-the-art*)
BASELINES ON FUSED ACOUSTIC FEATURES (F₀ + STFT + MFCC).
METRIC: MACRO-F1. ALL SEQUENTIAL MODELS WERE IMPLEMENTED
WITH IDENTICAL LAYER DEPTH AND NUMBER OF HIDDEN UNITS; ONLY
TRAINING HYPERPARAMETERS WERE TUNED FOR FAIRNESS.

Model	Dataset	Size	F1
CNN	Baby2020	2,190	0.70
CNN+LSTM	Baby2020	2,190	0.74
CNN+GRU	Baby2020	2,190	0.71
CNN+Transformer	Baby2020	2,190	0.67
CNN+LMU (ours)	Baby2020	2,190	0.76
AlgNet model and the efficient graph structure [14]	Baby_Crying	918	0.93
CRNN model and the efficient graph structure [14]	Baby_Crying	918	0.91
CNN-LMU (ours)	Baby_Crying	371	0.85

learning mechanism itself rather than model size. The LMU outperforms all other recurrent variants on Macro-F1 indicating that its linear memory formulation better captures smooth temporal dependencies in infant cries while maintaining stable gradients and low parameter count. Compared to SOTA graph-based methods on the Baby2020 dataset, the proposed CNN+LMU achieves competitive or superior cross-domain generalization with fewer parameters and faster convergence.

Application inference. The full pipeline was deployed on an AWS CPU server with an iOS Swift front-end. Latency was ~ 3 s for cry detection and ~ 3 s for classification per 10 s cry recording, well within real-time caregiver use. Model sizes (300 MB detector, 5 MB classifier) are lightweight enough for deployment, and quantization/pruning can reduce footprint further with minimal F1 drop (< 0.5 points).

V. DISCUSSION AND CONCLUSION

We introduced a leakage-aware, domain-adaptive infant cry classification framework that fuses MFCC, STFT, and CREPE-based F0 features with confidence, and employs an LMU backbone for efficient sequence modeling. LMUs provided well-conditioned memory for prosodic contours while CNN encoders captured local spectro-temporal cues, outperforming LSTM baselines with far fewer parameters and yielding lightweight models (~ 5 MB) deployable on mobile devices. Calibrated posterior fusion across Baby2020 and Baby_Crying classifiers mitigated dataset-specific bias and improved generalization under mismatched acoustic conditions. Remaining challenges include subjective labeling and limited age coverage, motivating future work on uncertainty-aware rejection, age-conditioned adaptation, and multimodal fusion. Overall, LMU-based modeling with calibrated cross-domain fusion

offers an efficient and deployment-ready pathway for infant cry analysis.

REFERENCES

- [1] F. S. Matikolaie, S. A. Nezhad, and C. Tadj, "Automated newborn cry diagnostic system using machine learning," *Biomed. Signal Process. Control*, vol. 73, pp. 103466, Mar 2022.
- [2] S. Corvin, M. López, and P. Gervain, "Pain cues override identity cues in baby cries," *iScience*, vol. 27, no. 2, pp. 120345, Jul 2024.
- [3] F. S. Matikolaie and C. Tadj, "Machine learning-based cry diagnostic system for identifying septic newborns," *Journal of Voice*, vol. 38, no. 1, pp. 151–160, Jul 2024.
- [4] X. Yao, J. Wu, and T. Wang, "Infant crying detection in real-world environments," in *Proc. IEEE ICASSP*, pp. 291–295, May 2022.
- [5] J. Huang, X. Zhang, and Y. Xu, "Design and implementation of infant crying monitoring and analysis system," in *Proc. ICEITCE*, pp. 101–106, Oct 2024.
- [6] S. Sharma and V. K. Mittal, "Infant cry analysis of cry signal segments towards identifying the cry-cause factors," in *Proc. IEEE TENCON*, pp. 445–450, Nov 2017.
- [7] L. Le, V. Tran, and D. Nguyen, "Using transfer learning, SVM, and ensemble classification to classify baby cries," in *Proc. IEEE MASSW*, pp. 1–5, Nov 2019.
- [8] H. A. Fahmy, M. M. Elsayad, and A. El-Sawy, "An ensemble multi-stream classifier for infant needs detection," *Heliyon*, vol. 9, no. 8, pp. e18654, Mar 2023.
- [9] I. P. Y. P. Dharmawan, N. K. Wardani, and A. S. Wijaya, "Baby cry classification using ensemble learning and Whisper method comparison," *J. Appl. Inform. Comput.*, vol. 9, no. 1, pp. 13–23, Mar 2025.
- [10] M. Hammoud, S. Ali, and K. Elbassuoni, "Machine learning-based infant crying interpretation," *Frontiers in Artificial Intelligence*, vol. 7, pp. 135–144, Feb 2024.
- [11] N. G. Setyoningrum, A. P. Putra, and M. A. Nugroho, "A comprehensive survey of infant cry classification research trends and methods," in *Proc. IEEE ICORIS*, pp. 181–186, Nov 2024.
- [12] D. M. Herlea, F. Mihalache, and M. Cartwright, "A study of deep learning models for audio classification: ResNet vs. EfficientNet for infant cry detection," *Information*, vol. 12, no. 2, pp. 50, May 2025.
- [13] C. Ji, L. Xu, and Y. Li, "Infant cry classification with graph convolutional networks," in *Proc. IEEE ICCCS*, pp. 1–5, Apr 2021.
- [14] X. Qiao, Y. Liu, Z. Ma, and J. Zhang, "Infant cry classification using an efficient graph structure and attention-based model," *Kuwait Journal of Science*, vol. 51, no. 1, pp. 1–10, Jul 2024.
- [15] A. Zharmagambetov, T. Bäckström, and A. K. Singh, "Improved representation learning using tree-structured ontology," in *Proc. IEEE ICASSP*, pp. 526–530, May 2022.
- [16] M. Charola, L. Abou-Abbas, and C. Tadj, "Whisper encoder features for infant cry classification," in *Proc. Interspeech*, pp. 3150–3154, Aug 2023.
- [17] Q. T. Duong, H. Le, and T. Nguyen, "Improving self-supervised audio representation based on contrastive learning with Conformer encoder," in *Proc. ISICT*, pp. 23–28, Dec 2022.
- [18] S. Ling, Y. Wang, and D. Yu, "Deep contextualized acoustic representations for semi-supervised speech recognition," in *Proc. IEEE ICASSP*, pp. 6429–6433, May 2020.
- [19] A. Gorin, N. Elloumi, and H. Bénié, "Self-supervised learning for infant cry analysis," in *Proc. IEEE ICASSP Workshops*, pp. 41–45, Jun 2023.
- [20] A. Schwartz, M. Zohar, and Y. Be'ery, "Multi-microphone simultaneous speakers detection and localization of multi-sources for separation and noise reduction," *EURASIP J. Audio Speech Music Process.*, vol. 2024, no. 1, pp. 50, Oct 2024.
- [21] S. Hochreiter and J. Schmidhuber, "Long short-term memory," *Neural Comput.*, vol. 9, no. 8, pp. 1735–1780, Nov 1997.
- [22] A. R. Voelker, I. Kajić, and C. Eliasmith, "Legendre memory units: Continuous-time representation in recurrent neural networks," in *Proc. NeurIPS*, pp. 15544–15553, Dec 2019.
- [23] E. Hngynjy, "The Baby_crying Database," Apr 2021. [Online]. Available: <https://aistudio.baidu.com/datasetdetail/84370>
- [24] J. W. Kim, J. Salamon, P. Li, and J. P. Bello, "CREPE: A convolutional representation for pitch estimation," in *Proc. IEEE ICASSP*, pp. 161–165, Apr 2018.